Optical absorption intensities and fluorescence dynamics of Ho^{3+} ions in $LiNbO_3$

1996 J. Phys.: Condens. Matter 8 5781

(http://iopscience.iop.org/0953-8984/8/31/011)

J. Phys.: Condens. Matter **8** (1996) 5781–5791. Printed in the UK

Optical absorption intensities and fluorescence dynamics of Ho^{3+} ions in $LiNbO_3$

A Lorenzo, L E Bausá, J A Sanz Garcia and J Garcia Solé

Departamento de Física de Materiales C-IV, Universidad Autónoma de Madrid, Cantoblanco, 28049-Madrid, Spain

Received 15 January 1996

Abstract. Optical absorption and fluorescence spectra have been systematically investigated in Ho^{3+}-doped $LiNbO_3$ crystals. The energy position and symmetry character of the Stark levels in the near-infrared region are deduced. The room-temperature absorption line strengths have been experimentally determined and the theory of Judd and Ofelt is used to obtain the radiative lifetimes and branching ratios of the emitting $^5S_2 + {}^5F_4$ and $^5F_5$ states. Non-radiative relaxation processes are found to contribute to the transition probabilities of both states. In the case of the $^5S_2 + {}^5F_4$ multiplets, a multiphonon relaxation process with an effective phonon energy of 559 cm^{-1} accounts for the temperature dependence of the lifetime. The $^5F_5$-state luminescence shows a non-exponential decay time which indicates the existence of an energy transfer process. This energy transfer process exhibits a Boltzmann-type temperature dependence and is attributed to two-phonon-assisted energy transfer.

1. Introduction

In the last few decades, a great effort has been made in the study of $LiNbO_3$, mainly owing to its excellent acousto-optic and electro-optic coefficients. This has revealed $LiNbO_3$ as a good candidate for optoelectronic devices. Moreover, the possibility of doping with rare-earth ions of the order of a few per cent has opened the door to new laser materials [1]. Combination of this feature with the non-linear properties of the $LiNbO_3$ matrix has permitted the development of $LiNbO_3$:MgO:Nd minilasers which exhibit self-frequency doubling, self-Q-switching and self-mode-locking [2, 3]. MgO codoping is necessary to avoid photorefractive damage [4].

$LiNbO_3$ is one of the matrices in which Ho^{3+} ions have been lased [1]. Holmium-doped systems appear interesting because of the laser emission obtained at around 2.1 μm [5–7]. However, although the optical properties of Ho^{3+} ions have been extensively studied for a variety of solid state matrices, the information on the $LiNbO_3$:Ho^{3+} system is scarce. Detailed spectroscopic analysis is thus necessary to know the capabilities and limitations of this laser system. In previous work by the present authors [8] the absorption spectra were studied at low temperatures in the visible region. The polarization character and energy position of most Stark levels in this spectral region have been demonstrated. Site-selective spectroscopy has also been used to demonstrate the existence of at least two optically non-equivalent Ho^{3+} centres. These centres have been interpreted by Rutherford back-scattering spectrometry–channelling experiments, as Ho^{3+} ions occupying Li^+ octahedra and displaced from the regular Li^+ position [9].

0953-8984/96/315781+11$19.50

In this work, we complete our previous results by studying the absorption bands in the near-infrared region and two luminescence channels in the visible region ($^5S_2 + {}^5F_4 \rightarrow {}^5I_7$ and $^5F_5 \rightarrow {}^5I_8$) not previously reported. Polarized optical absorption spectra at room temperature have been analysed and fitted using the theory of Judd [10] and Ofelt [11] (JO). The results of the JO calculation are then used to obtain information about the radiative lifetimes and spontaneous emission probabilities of the $^5S_2 + {}^5F_4$ and $^5F_5$ states. The temperature dependences of the lifetimes values are accounted for by considering multiphonon relaxation and phonon-assisted energy transfer processes.

2. Experimental details

The sample used in this work has been grown in our laboratory by the balance-controlled Czochralski method from grade I Johnson Matthey powder containing 1 mol% Ho^{3+} ions relative to Nb^{5+} ions. The crystal was prepared from a stoichiometric composition of the melt ([Li]/[Nb] = 1). Plates were cut and oriented using x-ray diffraction patterns to obtain samples with their faces parallel or perpendicular to the ferroelectric *c* axis. Polarized absorption spectra were obtained with the electric field of the incident beam perpendicular or parallel to the *c* axis (σ and π configurations, respectively). For these measurements a Hitachi U-3501 spectrophotometer and a calcite polarizer were used.

For the luminescence spectra, the third harmonic of a pulsed Nd:YAG laser was used as the excitation source. The signal was detected with a multialkali photon counter photomultiplier and gated techniques. A closed-cycle helium cryostat provided with a temperature controller was used to study the temperature dependences.

3. Results and discussion

3.1. Absorption spectra

The previous work reporting the optical spectra of $LiNbO_3$:Ho^{3+} was performed on congruent samples [8]. In this work, a nearly stoichiometric crystal ([Li]/[Nb] equal to 1 in the melt) was used, and so the effect of the intrinsic defects of the matrix on the optical properties of the Ho^{3+} ions can be envisaged.

The low-temperature (15 K) absorption spectra obtained in this stoichiometric sample are depicted in figure 1(a) and can be well compared with those obtained for the case of congruent samples ([Li]/[Nb] = 0.945) [8]. The only difference observed is that the linewidths are narrower than in the latter case. This is in agreement with results from other rare-earth-doped $LiNbO_3$ crystals, in which the main effect of varying stoichiometry is a reduction in the spectral bandwidth of optical transitions, as the Li-to-Nb ratio approaches unity [12]. This can be related to a lower number of intrinsic defects in the matrix.

However, the numbers of absorption lines, the energy positions and the relative intensities are exactly the same for both compositions. Thus, for this reason, the results obtained in this paper related to the identification of energy levels and fluorescence dynamics can also be applied to the congruent $LiNbO_3$:Ho^{3+} crystals.

The study of the absorption spectra in the near-infrared region provides new information that permits us to complete the spectroscopic characterization started in the previous work [8], as well as to increase the reliability of the JO parameters. Figure 1 shows the complete σ- and π-polarized absorption spectra of $LiNbO_3$:Ho^{3+} at a low temperature. A detailed analysis of the polarized spectra (including the α-polarized spectrum, which is identical with the σ-polarized spectrum) determined that all the transitions detected had a forced electric

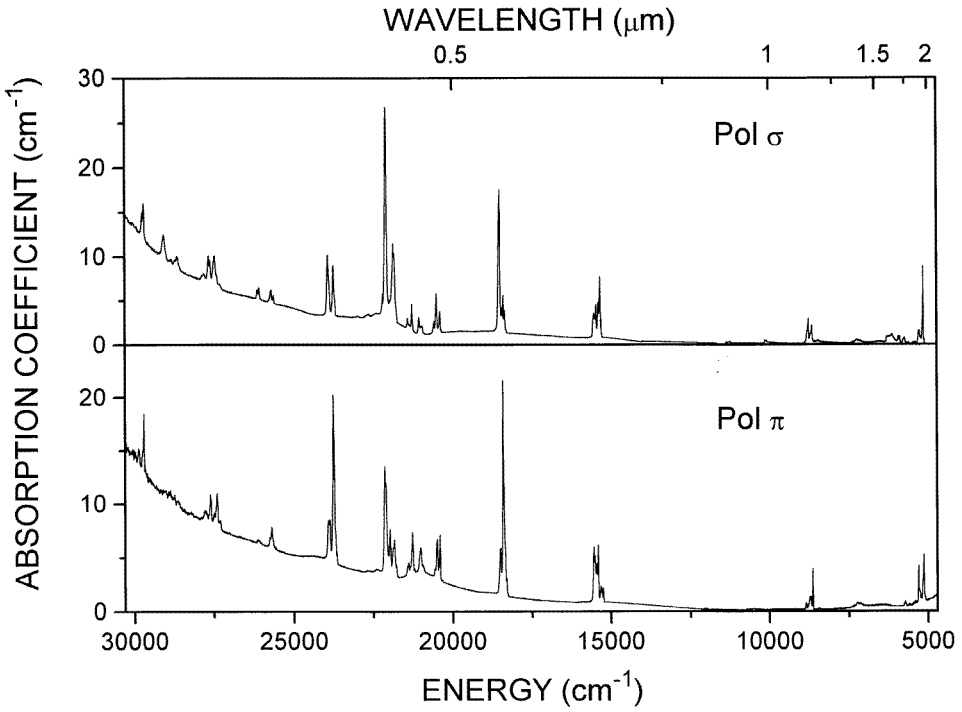

Figure 1. Absorption spectra of $LiNbO_3$:Ho^{3+} (1 mol% in σ and π configurations at a low temperature.

dipole character. Moreover, the polarization character of the ground Stark level was also inferred as A, in agreement with previous results [8]. By using the selection rules for electric dipole transitions in C_3 local symmetry (see table 1), the energy positions and symmetry character (E or A) of the Stark levels associated with the $^5I_5$, $^5I_6$, $^5I_7$ and $^5I_8$ states are determined in this work. These are listed in table 2. The energies of the $^5I_8$ ground-state Stark levels, not previously reported, are obtained from the $^5S_2 + {}^5F_4 \rightarrow {}^5I_8$ emission transition (see below) and are also included in table 2. The energy values of the $^5I_8$ and $^5I_7$ Stark sublevels are in agreement with previous results from Johnson and Ballman [1].

Table 1. Selection rules for electric dipole transitions.

	A	E
A	π	α, σ
E	α, σ	α, σ, π

3.1.1. Judd–Ofelt calculation The JO theory has been used in order to estimate the radiative lifetimes and transition probabilities. As $LiNbO_3$ is a uniaxial crystal, anisotropic effects must be considered, and thus polarized absorption spectra are needed. Room-temperature polarized absorption spectra have been obtained from 2000 to 300 nm for 1 mol% Ho^{3+}-doped $LiNbO_3$ and are shown in figure 2. The $^5I_7$ state will not be considered because it

Table 2. Energy levels and symmetry character of the infrared multiplets of $LiNbO_3$:Ho^{3+}.

Multiplet	λ (nm)	F (cm^{-1})	Symmetry character
$^5I_5$	880.0	11 363	E
	882.7	11 328	A
	885.2	11 296	E
	887.8	11 263	A
	888.9	11 249	E
$^5I_6$	1126.5	8 877	A
	1128.0	8 865	A
	1134.9	8 810	E
	1139.9	8 772	E
	1142.0	8 756	A
	1146.0	8 726	A
	1148.0	8 710	E
	1154.1	8 665	E
	1154.5	8 661	A
$^5I_7$	1882.5	5 312	A
	1890.0	8 291	E
	1901.5	8 259	E
	1911.0	5 232	A
	1928.5	5 185	A
	1932.2	5 174	A
	1937.1	5 162	A
	1943.6	5 145	E
	1947.5	5 134	E
	1957.1	5 109	E
$^5I_8$		422	
		387	
		342	
		303	
		270	
		237	
		195	
		69	
		42	
		8	
		0	A

might contain an important magnetic dipole contribution, according to the selection rules in the J quantum number.

From the area under these spectra, the integrated absorbances Γ for each transition were obtained as

$$\Gamma_p = \int \alpha(\lambda)\,\mathrm{d}\lambda \tag{1}$$

p being the polarization degree σ or π.

Hereafter, any anisotropic magnitude will be calculated as one third of the π component plus two thirds of the σ component [13]. Thus, for the integrated absorbance we have

$$\Gamma = \tfrac{1}{3}\Gamma_\pi + \tfrac{2}{3}\Gamma_\sigma. \tag{2}$$

Once we have the integrated absorbance Γ, the line strength S can be experimentally

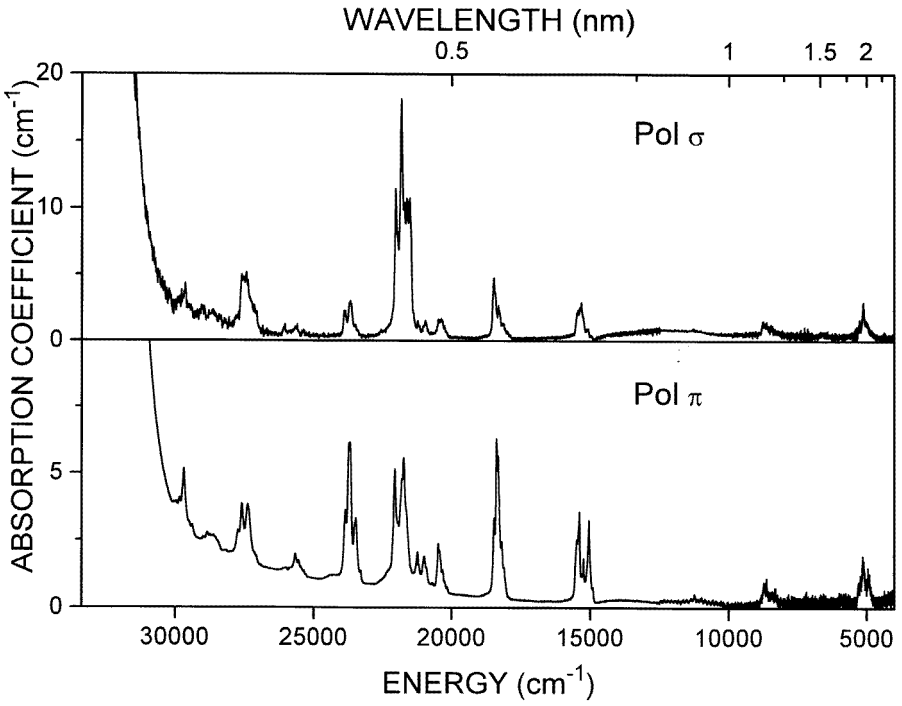

Figure 2. Room-temperature polarized absorption spectra of $LiNbO_3$:Ho^{3+} (1 mol%).

determined for each particular transition $J \rightarrow J'$ according to the formula

$$S(J,\ J') = \frac{3\mathrm{ch}(2J+1)}{8\pi^3 N \bar{\lambda}^3 \chi}\Gamma \tag{3}$$

where N is the Ho^{3+} concentration, $\bar{\lambda}$ is the mean transition wavelength and J is the total angular momentum quantum number of the initial manifold ($J = 8$ in our case). The Lorentz field correction χ is an anisotropic magnitude too, its components being

$$\chi_{\sigma,\pi} = \left(n_{\sigma,\pi}^2 + 2\right)^2 / 9n_{\sigma,\pi} \tag{4}$$

where n_σ and n_π are the ordinary and extraordinary refractive indices of $LiNbO_3$, evaluated for each value of $\bar{\lambda}$ [14].

In the JO theory, the line strength for the electric dipole transition is expressed as a sum of products of the matrix elements of unit tensor operators $U^{(t)}$ of rank t times the phenomenological parameters Ω_2 Ω_4 and Ω_6

$$S_{ed} = \sum_t \Omega_t \left|\langle SLJ||U^{(t)}||S'L'J'\rangle\right|^2 \ (t = 2,\ 4,\ 6). \tag{5}$$

Now the JO intensity parameters Ω_2, Ω_4 and Ω_6 can be determined by a least-squares fitting of the $S(J,\ J')$-values obtained experimentally, if the $|\langle SLJ||U^{(t)}||S'L'J'\rangle|^2$ matrix elements are known. These elements were taken from Rauber [14]. The intensity parameters obtained in such a fitting are $\Omega_2 = 4.30 \times 10^{-20}$ cm^2, $\Omega_4 = 5.11 \times 10^{-20}$ cm^2 and $\Omega_6 = 1.89 \times 10^{-20}$ cm^2, with a root mean square (rms) of 0.88×10^{-20} (relative error of

16.3%), which are comparable with those found in other Ho^{3+}-doped systems [15, 16]. The experimental and fitted values are listed in table 3.

Table 3. Experimental and fitted values of the line strengths for the absorption transitions of Ho^{3+} ions in $LiNbO_3$. $\Omega_2 = 4.3 \times 10^{-20}$ cm^2, $\Omega_4 = 5.11 \times 10^{-20}$ cm^2 and $\Omega_6 = 1.89 \times 10^{-20}$ cm^2. The RMS is 0.88×10^{-20} and the relative error is 16.3%.

Transition	Wavelength (nm)	S_{exp} (10^{-20} cm^2)	S_{calc} (10^{-20} cm^2
$^5I_8 \rightarrow\ ^5I_6$	1150	1.82	1.54
$^5I_8 \rightarrow\ ^5I_5$	890	0.31	0.23
$^5I_8 \rightarrow\ ^5F_5$	650	2.39	3.26
$^5I_8 \rightarrow\ ^5S_2 +\ ^5F_4$	545	2.62	1.48
$^5I_8 \rightarrow\ ^5F_3$	490	0.59	0.65
$^5I_8 \rightarrow\ ^5G_6 +\ ^5F_1 +\ ^5F_2 +\ ^3K_8$	406	9.90	9.90
$^5I_8 \rightarrow$	421	1.72	0.74

Once the intensity parameters have been determined, the electric dipole radiative transition probabilities $A_{ed}(J,\ J')$ from emitting levels can be estimated as

$$A_{ed}(J,\ J') = \frac{64\pi^4 e^2 \xi}{3h(2J+1)9\bar{\lambda}^3} S(J,\ J') \tag{6}$$

with $\xi = \frac{2}{3}\xi_\sigma + \frac{1}{3}\xi_\pi$ and

$$\xi_{\sigma,\pi} = n_{\sigma,\pi}\left(n_{\sigma,\pi}^2 + 2\right)^2. \tag{7}$$

Then, the radiative lifetimes $\tau_r = 1/\sum A(J,\ J')$ have been obtained for the emitting $^5S_2$, $^5F_4$ and $^5F_5$ levels. These values are included in table 4.

Table 4. Calculated spontaneous emission probabilities for $LiNbO_3$:Ho^{3+} for the emitting $^5S_2$, $^5F_4$ and $^5F_5$ states.

Transition	Wavelength (nm)	Transition probability (s^{-1})		Radiative lifetime (μs)
$^5S_2$ ($^5F_4$) $\rightarrow\ ^5F_5$	3360	2.40	(27.96)	109.2 (46.3)
$^5S_2$ ($^5F_4$) $\rightarrow\ ^5I_4$	1901	153.84	(77.99)	
$^5S_2$ ($^5F_4$) $\rightarrow\ ^5I_5$	1375	138.32	(537.80)	
$^5S_2$ ($^5F_4$) $\rightarrow\ ^5I_6$	1017	619.67	(1428.17)	
$^5S_2$ ($^5F_4$) $\rightarrow\ ^5I_7$	757	3082.94	(2387.87)	
$^5S_2$ ($^5F_4$) $\rightarrow\ ^5I_8$	543	5161.35	(17161.24)	
$^5F_5 \rightarrow\ ^5I_4$	4378	0.30		79.2
$^5F_5 \rightarrow\ ^5I_5$	2327	27.16		
$^5F_5 \rightarrow\ ^5I_6$	1459	373.01		
$^5F_5 \rightarrow\ ^5I_7$	973	2405.25		
$^5F_5 \rightarrow\ ^5I_8$	648	9813.50		

3.2. Fluorescence dynamics

The fluorescence of $LiNbO_3$:Ho^{3+} in the visible region mainly consists of emissions from the metastable $^5S_2 +\ ^5F_4$ and $^5F_5$ states. Three bands centred at 550 nm, 760 nm and

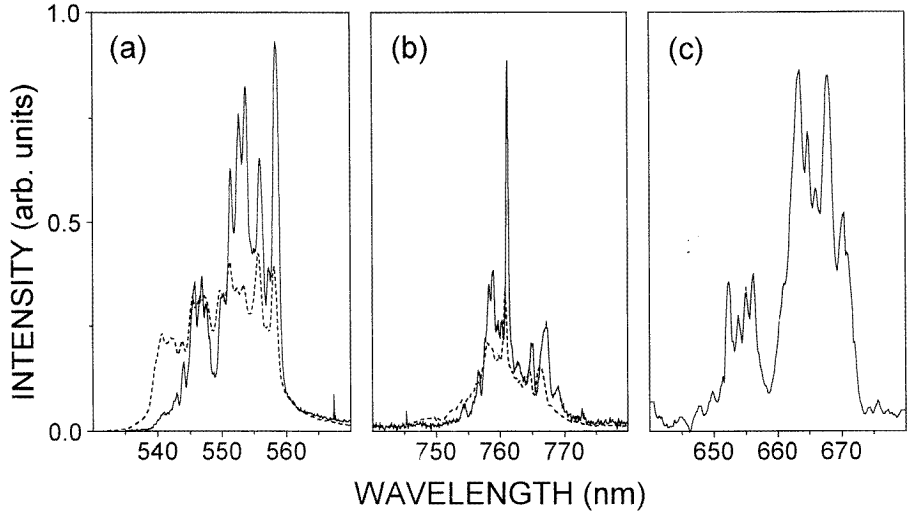

Figure 3. Luminescence spectra of $LiNbO_3$:Ho^{3+} in the visible region: (a) $^5S_2 + {}^5F_4 \rightarrow {}^5I_8$; (b) $^5S_2 + {}^5F_4 \rightarrow {}^5I_7$; (c) $^5F_5 \rightarrow {}^5I_8$. In (a) and (b) the room-temperature spectra are also drawn as broken curves.

660 nm were detected and assigned to the transitions $^5S_2 + {}^5F_4 \rightarrow {}^5I_8$, $^5S_2 + {}^5F_4 \rightarrow {}^5I_7$ and $^5F_5 \rightarrow {}^5I_8$, respectively. These spectra are shown in figure 3.

3.2.1. $^5F_4 + {}^5S_2$ *luminescence dynamics.* As occurs in many other Ho^{3+}-doped materials, the energies of the $^5S_2$ and $^5F_4$ states are so close that the populations of these states are in a thermal equilibrium and, when the temperature is increased, the contribution from the upper $^5F_4$ multiplet could be important. This can be observed in figures 3(a) and 3(b) when comparing the low-temperature and room-temperature spectra.

The transition probability from the $^5F_4$ state to the $^5I_8$ multiplet is higher than from the $^5S_2$ state (see table 3), and thus, when the temperature increases, the high-energy part of the spectrum (see figure 3(a)) becomes important.

On the other hand, the $^5F_4 \rightarrow {}^5I_7$ emission probability is smaller than the $^5S_2 \rightarrow {}^5I_7$ probability (see table 3), and no significant broadening is observed in the high-energy part of the spectrum (see figure 3(b)).

The energy separation E between the $^5F_4$ and the $^5S_2$ states can be roughly estimated by taking into account the emission intensity ratio terminating in the $^5I_7$ and $^5I_8$ states. By using a simple four-level model [15] including the $^5F_4$ (level 1), $^5S_2$ (level 2), $^5I_7$ (level 3) and $^5I_8$ (level 4) states, the ratio of the $^5S_2 + {}^5F_4 \rightarrow {}^5I_7$ integrated intensity to the $^5S_2 + {}^5F_4 \rightarrow {}^5I_8$ integrated intensity as a function of temperature is given by

$$\frac{I_7}{I_8} = \frac{C_7(\nu)h\nu_7\, 9A_{13}\ \exp^{(-E/kT)} + 5A_{23}}{C_8(\nu)h\nu_8\, 9A_{14}\ \exp^{(-E/kT)} + 5A_{24}} \tag{8}$$

where A_{ij} is the emission probability from table 3, for a transition between i and j levels. C_7 and C_8 represent the correction factors of the detector for each spectral range.

When $T \approx 0$ the $^5F_4$ state is not thermalized, and the above expression yields a value of 0.17, which is very similar to the experimental value obtained from the areas of the spectra: 0.15. Fitting the experimental values to equation (8), for temperatures ranging

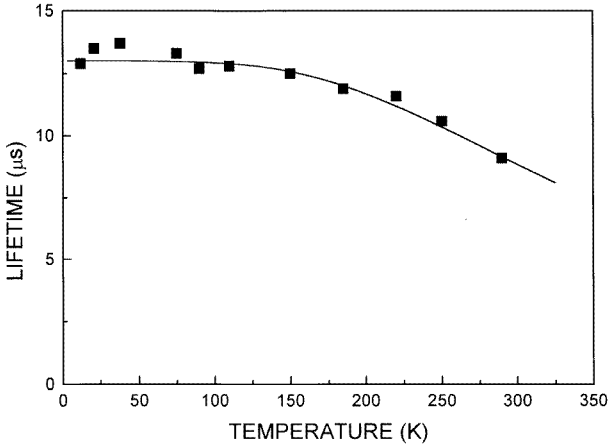

Figure 4. Temperature dependence of the $^5S_2 + {}^5F_4$ fluorescence lifetime. The solid curve represents the best fit to the experimental data.

from 15 to 300 K, the energy gap E between the $^5F_4$ and $^5S_2$ manifolds is found to be around 200 cm^{-1}, which is in agreement with the data reported for Ho^{3+} in other hosts [15–18].

The temperature dependence of the fluorescence lifetimes from the $^5S_2 + {}^5F_4$ state is plotted in figure 4. The decay curves were single exponential for all the temperatures studied and the lifetime decreased from 14 to 9 μs with increasing temperature. This behaviour is mainly due to a non-radiative multiphonon relaxation which dominates the transition probability of the $^5S_2 + {}^5F_4$ state because of the small energy difference from the low-lying $^5F_5$ state (2480 cm^{-1}). The most accurate expression to account for the temperature dependence of a multiphonon relaxation involving p phonons is [19]

$$W_{nr} = W_{nr}(0)\left(1 + n_{eff}\right)^p \tag{9}$$

where n_{eff} is the occupancy of the effective phonon modes given by

$$n_{eff} = \left(\exp\left(\hbar\omega_{eff}/kT\right) - 1\right)^{-1}. \tag{10}$$

However, thermalization of the $^5F_4$ state must also be considered in the expression for the radiative rate according to

$$W_r = \left[9\sum A\left({}^5F_4\right)\ \exp\left(-\frac{E}{kT}\right) + 5\sum A\left({}^5S_2\right)\right] \Big/ \left[9\ \exp\left(-\frac{E}{kT}\right) + 5\right] \tag{11}$$

where E is the energy separation between the $^5S_2$ and $^5F_4$ states, previously estimated as 200 cm^{-1}. The experimental data in figure 4 are then fitted to the following expression:

$$\frac{1}{\tau} = W_r + W_{nr}. \tag{12}$$

As a result, values of $W_{nr}(0) = 70\,407$ s^{-1}, $E = 214$ cm^{-1} and $p = 5.08$ are obtained. This value of p indicates that the energy of the effective phonon is 559 cm^{-1}. This is not the highest-energy phonon available in the $LiNbO_3$ lattice but, in the Raman spectra, an intense peak at 580 cm^{-1} appears [20].

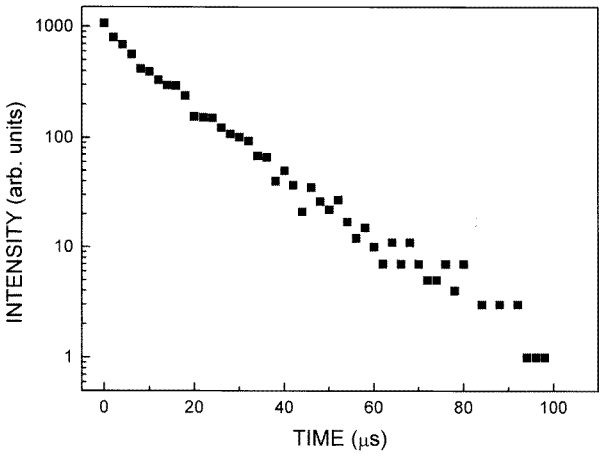

Figure 5. Non-exponential decay curve of the $^5F_5$ state at 15 K.

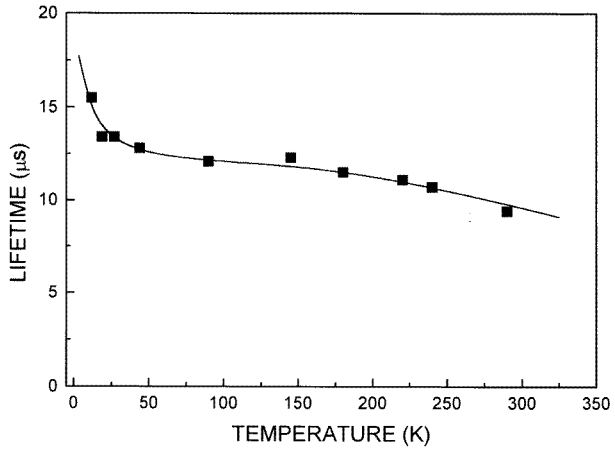

Figure 6. Temperature dependence of the $^5F_5$ fluorescence lifetime. The solid line represents the best fit to equation (12).

3.2.2. $^5F_5$ *luminescence dynamics.* Conversely to the behaviour of the $^5F_4 + {}^5S_2$ state, the decay curves of the $^5F_5$ multiplet exhibited a slightly non-exponential behaviour, as can be seen in figure 5. This indicates the existence of a short-range energy transfer process. In addition, if we consider an effective lifetime value, we observe a decrease from 15 to 9 μs on increasing the temperature from 15 to 300 K.

The temperature dependence of the $^5F_5$ lifetime is plotted in figure 6. For the low-temperature range ($T < 50$ K), multiphonon relaxation is negligible and the values of the lifetime are found to follow an exponential dependence on temperature, as would correspond to a temperature-dependent energy transfer process:

$$W_{ET} = W_{ET}(0)\ \exp(-\delta/kT) \tag{13}$$

where W_{ET} is the energy transfer probability, $W_{ET}(0)$ is the energy transfer probability at 0 K and δ is an activation energy for the transfer process.

For the high-temperature range, multiphonon relaxation becomes important and equation (9) can be used to fit the decay time values.

The plot in figure 6 is then fitted to an expression containing both processes: the temperature-dependent energy transfer and the non-radiative multiphonon relaxation. The radiative lifetime obtained from the JO calculation has also been considered. If we put the energy of the effective phonon involved in the multiphonon relaxation equal to $\bar{h}\omega = 559$ cm^{-1}, we obtain a value for the transfer activation energy $\delta = 8.6$ cm^{-1}.

The temperature dependence of the energy transfer rate clearly indicates that this process is phonon assisted. This energy transfer could occur between two near Ho^{3+} ions with some mismatch between their energy levels. A different crystalline environments could account for the small difference in the energy levels. In fact, the presence of two non-equivalent Ho^{3+} centres in $LiNbO_3$ was evidenced by site-selective spectroscopy [8].

Once we have determined the existence of phonon-assisted energy transfer, the temperature dependence of the $^5F_5$-state lifetime allows us to discuss the nature of the process. The exponential behaviour observed at low temperatures indicates that two phonons must be involved [21]. This is expected when the energy mismatch is small and the distance between ions is not too large.

Among the variety of two phonon-assisted energy transfer processes, the more common dependences are T^3, T^7 and $\exp(-\delta/kT)$. The exponential dependence is attributed to a process in which an additional electronic level of the ion (at an energy distance δ from any of the involved levels) participates in the process. In the case of Ho^{3+} ions in $LiNbO_3$, this level could be the first excited level of the $^5I_8$ ground state which is located at a bout 8 cm^{-1} (see table 2), in agreement with the estimated value of $\delta = 8.6$ cm^{-1}.

4. Conclusion

In this work, the optical absorption and emission spectra and the fluorescence dynamics of the $^5S_2 + {}^5F_4$ and $^5F_5$ states of $LiNbO_3Ho^{3+}$ have been systematically investigated.

First, the scheme of levels of the $LiNbO_2$:Ho^{3+} system has been completed with the characterization of the infrared multiplets: $^5I_8$, $^5I_7$, $^5I_6$ and $^5I_5$. Then, the oscillator strengths of all absorption transitions were well fitted using the JO theory, so that the intensity parameters $\Omega_2 = 4.30 \times 10^{-20}$ cm^2, $\Omega_4 = 5.11 \times 10^{-20}$ cm^2 and $\Omega_6 = 1.89 \times 10^{-20}$ cm^2 were obtained.

The radiative rates deduced from the JO calculation and the temperature dependences of the measured lifetimes have been used to investigate the fluorescence dynamics of the $^5F_4 + {}^5S_2$ and $^5F_5$ emitting states. In the former case, a multiphonon relaxation rate is found and explained with an effective phonon of 559 cm^{-1}. In the latter, the same multiphonon relaxation mechanism occurs together with a temperature-dependent energy transfer process. This process has been attributed to two-phonon-assisted transfer between two non-equivalent Ho^{3+} centres and described by a Boltzmann-type expression.

Acknowledgments

This paper has been supported by the Comisión Interministerial de Ciencia y Técnologia (CICYT) under project MAT 95/152. A Lorenzo holds a grant from Ministerio de Educación y Ciencia.

References

[1] Johnson L F and Ballman A A 1969 *J. Appl. Phys.* **40** 1
[2] Córdova-Plaza A, Digonnet M and Shaw H J 1987 *IEEE J. Quantum Electron.* **QE-13** 262
[3] Lallier E, Pocholle J P, Papuchon M, de Micheli M, Li J M, He Q, Ostrowski D B, Grezes-Besset D and Pelletier E 1990 *Opt. Lett.* **15** 682
[4] Zhong G G, Jian J and Wu Z K 1980 *Proc. 11th Int. Quantum Electronics Conf.* (New York: IEEE) p 631
[5] Bowman S R, Winings M J, Searles S and Feldman B J 1991 *IEEE J. Quantum Electron.* **QE-27** 1129
[6] Johnson L F and Guggenheim H J 1974 *IEEE J. Quantum Electron.* **QE-10** 442
[7] Storm M E and Deyst J P 1991 *IEEE Trans. Photonics Technol. Lett.* **3** 982
[8] Lorenzo A, Bausá L E and García Solé J 1994 *J. Phys.: Condens. Matter* **6** 1065
[9] Lorenzo A, Jaffrezic H, Roux B, Boulon G and García Solé J 1995 *Appl. Phys. Lett.* **67** 3735
[10] Judd B R 1962 *Phys. Rev.* **127** 750
[11] Ofelt G S 1962 *J. Chem. Phys.* **37** 511
[12] Lorenzo A, Bausá L E, Voda M and García Solé J 1994 *J. Physique IV Coll.* **4** C4 381
[13] Lomheim T S and DeShazer L G 1978 *J. Appl. Phys.* **49** 5517
[14] Rauber A 1978 *Current Topics in Materials Science* vol 1 ed E Kaldis (Amsterdam: North-Holland)
[15] Weber M J, Matsinger B H, Donlan V J and Surrat G T 1972 *J. Chem. Phys.* **57** 562
[16] Tanimura K, Shinn M D, Sibley W A, Drexhage M G and Brown R N 1984 *Phys. Rev.* B **30** 2429
[17] Karayianis N, Wortman D E and Jenssen H P 1976 *J. Phys. Chem. Solids* **37** 675
[18] Carnall W T, Fields P R and Rajnak K 1968 *J. Chem. Phys.* **49** 4424
[19] Riseberg L A and Moos H W 1968 *Phys. Rev.* **178** 429
[20] Claus R, Borstel G, Wisendanger E and Steffan L 1972 *Phys. Rev.* B **6** 4878
[21] Holstein T, Lyo S K and Orbach R 1981 *Laser Spectroscopy of Solids* ed W M Yen and P M Selzer (Berlin: Springer)